Centrifuge Modeling of LNAPL Infiltration in Granular Soil with Containment

Chusak Kererat[1]; Inthuorn Sasanakul, A.M.ASCE[2]; and Suttisak Soralump[3]

Abstract: This paper presents the results from four centrifuge experiments modeling light, nonaqueous phase liquid (LNAPL) migration in a sandy soil. These experiments were performed to evaluate the performance of a soil-cement wall used as a containment barrier and to investigate the effects of groundwater flow on LNAPL migration behavior. Centrifuge modeling experiments were performed at 30 g to simulate 80 days of LNAPL migration through the soil. Pore water pressure measurements and video recordings were used to evaluate the LNAPL migration behavior. Results show that in all tests, the water level was depressed because of the large volume of LNAPL confined between the walls. When groundwater flowed, the LNAPL migrated faster and deeper than when there was no groundwater flow. As a result, the depth of a soil-cement wall should be designed to a greater maximum depth to account for the groundwater-flow effects. In addition, numerical simulations were performed and validated with the centrifuge test results. Both methods showed a good agreement as they provided similar behavior of the LNAPL migration and confirmed the effective performance of the soil-cement wall as a containment barrier. **DOI: 10.1061/(ASCE)GT.1943-5606.0000754.**

CE Database subject headings: Centrifuge models; Sand (soil type); Cement; Infiltration; Granular media.

Author keywords: Centrifuge modeling; LNAPL migration; Sandy soil; Soil-cement barrier.

Introduction

Contamination in soil and groundwater is a growing public concern affecting human health and the environment. Numerous contaminant sources located in city and rural environments include gas stations, chemical manufacturing and processing facilities, farms, and other facilities that have aboveground storage tanks (ASTs) and underground storage tanks (USTs) to store chemicals and fuels. Many of these tanks have reached or exceeded their useful design life and are leaking materials. Many of the contaminants leaking from USTs are petroleum hydrocarbons that are nearly immiscible in water and are thus referred to as nonaqueous phase liquids (NAPLs). Light NAPLs (LNAPLs), which are lighter than water, travel through the vadose zone under the force of gravity. If a small volume of an LNAPL is released into the subsoil, the LNAPL will be retained by capillary forces in the soil pores and may migrate laterally. If a sufficient amount is released, the LNAPL may not only be retained in the soil pores but may also depress the capillary fringe and the groundwater. The retained NAPL can migrate laterally because some of the NAPL components can dissolve in the groundwater and move by diffusion and advection with groundwater flow. During the rainy season, rainfall can mobilize the LNAPL depending on the LNAPL saturation and pressure in vadose zone. The LNAPL can act as a long-term and persistent source of contamination through the slow dissolution of compounds in flowing rainwater or groundwater. To control migration of the LNAPL leaking from ASTs and USTs, and to minimize the risks to human health and the environment, many remediation methods have been developed. One of the common methods is containment, which is the main focus of this study.

Previous studies of LNAPL migration in subsurface soil have included laboratory studies, numerical simulations, and field investigations. All of these approaches have their limitations. Laboratory studies are easy to perform but cannot simulate stress conditions and the long-term monitoring of LNAPL migration. Numerical simulations have limitations because of the difficulty in developing realistic input parameters. Field investigations are costly and may require several years to collect the required data. The geotechnical centrifuge-modeling test is a great alternative to these methods because stress conditions can be simulated and long-term migration can be accelerated in the centrifuge. In addition, centrifuge tests are significantly less expensive than field investigations.

The basic principle of centrifuge modeling is that stress conditions in the small scale model must be the same as in the prototype under Earth's gravity field. For example, the water pressure profile under hydrostatic conditions in a prototype soil deposit with a thickness of H is ρ_w g $H(\gamma_w = \rho_w$ g, where ρ_w = water density). The equivalent Ng centrifuge model has a soil deposit with a thickness of H/N (N times smaller than the prototype). Considering the increase in the unit weight of water in the increased gravity field ($\gamma_w = \rho_w N$g), the pore water pressure profile at a distance of H/N from the water level is ρ_w g $H(\rho_w N$g $H/N)$. Thus, the water pressure in the centrifuge model will be identical to those in the prototype. When the same model is at 1 g, the water pressure profiles (ρ_w g H/N) are not the same as those of the prototype. The scale model tested in geotechnical centrifuge modeling can be extended to a prototype scale using scaling laws. Scaling relationships for contaminant transport problems were summarized by Garnier et al. (2007). Centrifuge modeling tests aim to reproduce identical stresses

[1]Doctoral Candidate, Dept. of Civil Engineering, Kasetsart Univ., Jatujak, Bangkok, Thailand 10900. E-mail: g4985008@ku.ac.th

[2]Research Assistant Professor, Geotechnical Centrifuge Research Center, Rensselaer Polytechnic Institute, Troy, NY 12180 (corresponding author). E-mail: sasani@rpi.edu

[3]Associate Professor, Dept. of Civil Engineering, Kasetsart Univ., Jatujak, Bangkok, Thailand 10900. E-mail: fengsus@ku.ac.th

Note. This manuscript was submitted on August 23, 2011; approved on July 10, 2012; published online on May 15, 2013. Discussion period open until November 1, 2013; separate discussions must be submitted for individual papers. This paper is part of the ***Journal of Geotechnical and Geoenvironmental Engineering***, Vol. 139, No. 6, June 1, 2013. ©ASCE, ISSN 1090-0241/2013/6-892–902/$25.00.

in a model and a corresponding prototype with a small-scale and accelerated modeling time. The stress condition is a result of the self-weight of the soil layer influencing three aspects of contaminant transport (Taylor 1995). First, the stress level affects material properties such as porosity and permeability that affect the movement of liquid contaminants through soil. Second, contaminant transport problems always occur under gravitational force. Third, geoenvironmental problems often involve flow in which capillary rise zones and total potential gradients are governed by gravity.

One of the earliest uses of the centrifuge in geoenvironmental research was by Arulanandan et al. (1988), who successfully modeled pollutant migration in saturated soil. Illangasekare et al. (1991) investigated the one-dimensional movement of LNAPLs through partially saturated soil following a surface spill under a gravitational force 20 times Earth's gravity. Esposito et al. (1999) simulated a two-dimensional (2D) LNAPL spill in loose and dense unsaturated sands to observe the progress of LNAPL under two gravity accelerations. Soga et al. (2003) investigated the movement and the entrapment of water and LNAPLs in unsaturated, layered-soil deposits and compared the results to those of a numerical simulation. Hayashi and Allersma (2004) observed LNAPL transportation by groundwater flow in a sand deposit, while taking the effect of an impervious wall installed in the sand layer into account. Lo et al. (2004) investigated the LNAPL migration pattern and the benzene, toluene, ethylbenzene, and xylenes (BTEX) concentration distributions in subsurface systems by taking the effects of soil type into account. Hu et al. (2006) modeled LNAPL migration in unsaturated soil and in-situ soil vapor extraction (SVE) remediation to evaluate the behavior of contamination and the effectiveness of the SVE method. All of these studies were performed using centrifuge-modeling techniques and have shown that centrifuge modeling can be used as a potential experimental tool for studying the behavior of LNAPL migration in unsaturated soil. These studies can be summarized as follows: LNAPL can displace the capillary fringe and the water table; the plume spreads more laterally in dense sand than in loose sand; the porosity influences both the residual LNAPL content and the contaminated volume; and the effect of the increase and the decrease of the water level affects the LNAPL lens that travels with the groundwater flow.

Several researchers (Gazaway and Jasperse 1992; Bruce 2000; Kererat and Chaikaew 2009a) suggested that soil-cement mixing could be used for containment and remediation systems in geoenvironmental applications. Currently, there is limited experimental data available on the behavior of LNAPL migration in sandy soil contained by soil-cement walls and the effect of groundwater flow on the wall performance.

The objective of this paper is to present the results of four centrifuge model experiments of LNAPL migration in sand contained by soil-cement walls and to compare these results with those obtained from numerical simulations. The effects of groundwater flow on the wall performance were investigated. All of the experiments were designed to represent the seasonal change in hydrogeology found in in Thailand. Two experiments were performed under no-groundwater flow conditions, representing the hot and the cool dry seasons. The other two experiments were performed under groundwater flow conditions, representing the rainy season during which groundwater is likely to flow to water resources, such as pumping wells, reservoirs, and rivers. Pore pressure sensors were installed in the centrifuge model at various locations to monitor water pressure changes during the experiments, and video recording was used to record the LNAPL plume migration during the centrifuge experiments.

Centrifuge Modeling Tests

Model Configuration

In this study, the centrifuge experiments were performed at 30 times the Earth's gravity (g) using the geotechnical centrifuge laboratory at Rensselaer Polytechnic Institute (RPI), in Troy, NY. More detailed information regarding the RPI centrifuge can be found at http://www.nees.rpi.edu.

A strongbox that is 0.370 m wide, 0.876 m long, and 0.356 m high, equivalent to the prototype dimensions of 11.10 m × 26.28 m × 10.68 m at 30 g, was used for the experimental program. The box consists of a 0.05-m thick front Plexiglas wall and 0.025-m thick aluminum plate for the remaining sides. The geometry of the models with model units at 1 g is shown in Fig. 1. Two soil-cement walls used for containment were constructed for both hydrogeologic conditions and were located 0.05 m (1.50 m in the prototype) from the spill point in both the left and right directions. Each wall was 0.02 m wide, 0.37 m long, and 0.20 m deep, equivalent to the prototype dimensions of 0.60 m × 11.10 m × 6.00 m at 30 g. The wall was extended above the sand layer 0.135 m to prevent LNAPL flow across the top of the wall. The total thickness of the sand deposit was 0.267 m (8.01 m in the prototype).

Experimental Materials

The sandy soil used in this study was Nevada sand, which is silica sand with a particle density of 2,650 kg/m^3, a maximum dry density of 1,709.14 kg/m^3, a minimum dry density of 1,513.74 kg/m^3, and a hydraulic conductivity range of 4.75 m/day to 1.99 m/day, depending on its relative density. Nevada sand is a uniformly graded soil with a mean grain size (D_{50}) of 0.15 mm. The coefficient of uniformity (C_u) and the coefficient of curvature (C_c) of Nevada sand are 2.056 and 0.894, respectively. In this experiment, the desired dry density of the soil was 1,600 kg/m^3, which corresponds to a relative density of 50% and a porosity of ~40%. The saturated hydraulic conductivity used for this sand was 5.6×10^{-3} cm/s.

As presented previously, the soil-cement walls used in this study were 0.02 m thick, 0.37 m wide, and 0.20 m deep. The desired thickness and dry density of the soil-cement wall in the prototype scale were 0.60 m and 1,740 kg/m^3, respectively. The walls were made from a mix of Nevada sand with portland cement and water using a water/cement ratio (w/c) of 2 and a cement content of 220 kg/m^3 as recommended by Nicholson et al. (1997), based on more than 25 projects on in-situ auger-type soil mixing and jet grouting. The soil-cement wall was comprised of a mixture of 2651.44 g, 367.84 g, and 735.68 g of Nevada sand, cement, and water, respectively. The permeability of this soil-cement mixture was assumed to be 1.4×10^{-7} cm/s based on tests conducted by Kererat and Chaikaew (2009a). After mixing, two soil-cement walls were constructed within the strongbox by casting the walls in place. Both ends of soil-cement wall were adhered to a rubber sheet and fixed to the sidewalls of the strongbox.

The LNAPL used in this experiment was paraffin liquid, selected for its very low volatility at room temperature and its negligible solubility in water and low health hazard risk (Kamon et al. 2006). To enhance the intensity of paraffin's red color, Sudan IV was used as a dye at a ratio of 0.1% by weight (Sripongphichit 2006). The properties of paraffin liquid, Sudan IV, and water are summarized in Table 1.

Groundwater Flow System

The groundwater flow system was designed and developed to investigate the effect of differential pressure head on the behavior of

J. Geotech. Geoenviron. Eng. 2013.139:892-902.

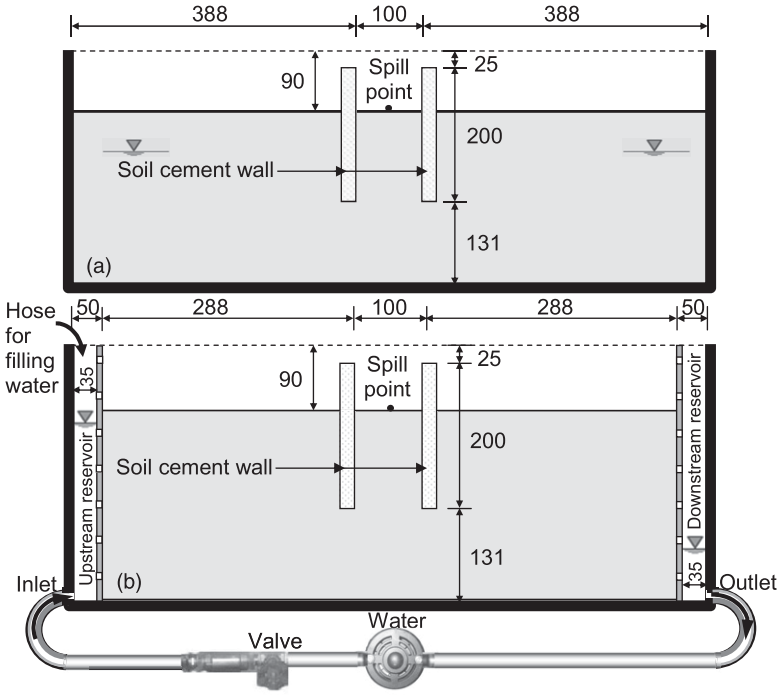

Fig. 1. Schematic diagram of strongbox; (a) no groundwater flow; (b) groundwater flow (model unit: mm)

Table 1. Properties of Paraffin Liquid, Sudan IV, and Water

Properties	Liquid paraffin	Sudan IV	Water
Formula	$C_{20}H_{42}$ (above)	$C_{24}H_{20}N_4O$	H_2O
Appearance	Colorless, odorless	Dark brown powder	Colorless, odorless
Boiling point	>300°C		100°C
Melting point	−18°C	199°C	0°C
Evaporation rate	Nonvolatile		
Solubility	Insoluble in water		
Viscosity	170 mPa s		
Hazard nature	Nontoxic		
Surface tension	31.07 mN/m		72.75 mN/m
Interfacial tension	62.06 mN/m		
Specific gravity	0.88 g/cm^3		0.998 g/cm^3

LNAPL migration. Fig. 1(b) presents the test setup for the groundwater flow case. To maintain the groundwater flow along the length of the model, a differential pressure was established by creating water reservoirs at both ends of the model. In these tests, the strongbox was divided into three sections using two 0.0127-m thick perforated walls made of aluminum and covered with geotextile. The sand deposit was contained in the center section of the strongbox, and the two side sections were used as water reservoirs to control the water table at the boundaries of the soil sample. The wall of the reservoir in contact with the soil was perforated uniformly with small holes to allow water to flow freely and evenly into the soil. A pump system was developed to collect water from the low-pressure reservoir (downstream) and return the water to the high-pressure supply reservoir (upstream). The flow rate of the pump was adjustable to allow the desired pressure differential in the two reservoirs to be set, thereby controlling the groundwater flow within the model. A separate water supply hose was also installed in the high-pressure reservoir. Furthermore, water could be added to the model through the centrifuge rotary joint to compensate for any evaporative loss during the experiment.

LNAPL Spill System

A special spill system developed for this study consisted of a container and a spill system. The container was 0.28 m in diameter and 0.15 m high and was welded to U-shaped steel bars mounted on the top of the strongbox by bolts. The spill system was developed to release the LNAPL to the soil surface at the center of the model container while the centrifuge was spinning at 30 g. At the beginning of the test, a closed solenoid valve held the LNAPL in the container. When the test was ready to run, the LNAPL was released through a very small interchangeable orifice. This system was tested extensively with various sizes and numbers of orifice holes to achieve the desired flow rate. In addition, the container was designed to have a large diameter and a minimum height to minimize the change in the flow rate through the orifice as the head in the container diminished. The LNAPL was released through the orifice at a constant rate and the flow rate was monitored using a pore-pressure sensor installed at the bottom of the LNAPL container.

Soil Preparation and Instrumentations

Dry sand was placed in the strongbox from a constant height using pluviation, also known as sand raining. The pluviation tool was made of sheet metal formed into a triangular funnel with a row of 1.6 mm holes at the bottom of the tool to release the sand. The pluviation tool was 15.25-cm wide and 15.9-cm high. Sand was poured into the top opening of the funnel and the device was moved in a smooth back and forth motion across the box to let the sand fall evenly into the box. Sand was pluviated lift by lift and pore-pressure sensors were placed at each lift. Details of the lift thicknesses and the locations of the sensors are shown in Fig. 2. The sand density in each lift was verified to ensure a uniform sand density throughout the model. After the dry sand preparation was completed, a predetermined amount of

J. Geotech. Geoenviron. Eng. 2013.139:892-902.

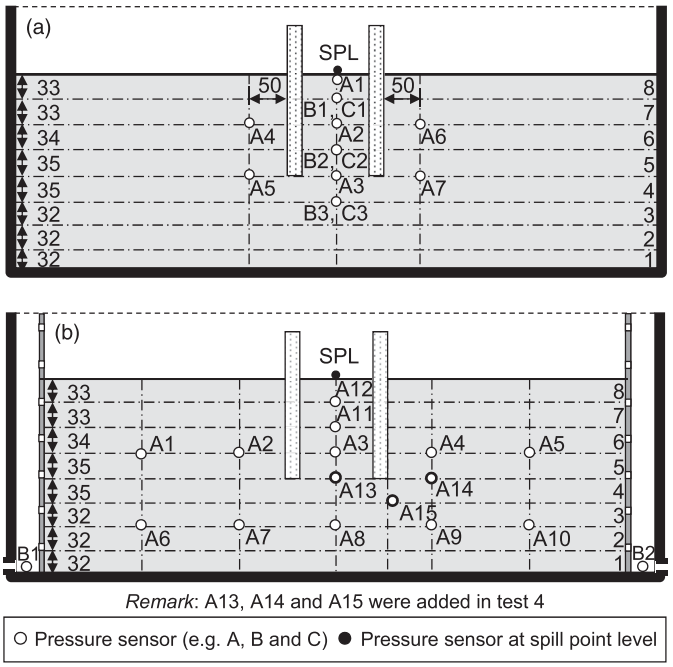

Fig. 2. Pressure sensor location; (a) no groundwater flow; (b) groundwater flow (model unit: mm)

water was gradually added to the sand until the water reached the desired level. This process was conducted by slowly dripping water into a sponge that was placed on the sand surface at a corner of the strongbox. The water level was monitored using pore-pressure sensors during the centrifuge spin up.

Initial Condition and Test Procedure

As mentioned previously, all of the experiments were performed at a centrifugal acceleration of 30 g. Tests 1 and 2 were under no groundwater flow conditions at various water levels. The phreatic surface of groundwater was 3.63 m and 1.81 m below the soil surface for tests 1 and 2, respectively, as shown in Fig. 3. The phreatic surface was developed from water pressure measured by pore-pressure sensors at various locations in the model.

Tests 3 and 4 were performed under groundwater flow conditions at 3.67 m and 6.49 m difference in head pressure, respectively, and the water level below the soil surface at the middle of the container was 2.20 m for test 3 and 2.72 m for test 4. The phreatic surfaces simulated by a numerical simulator program, *TMVOC*, were comparable with the measured values from pore-pressure sensors, as shown in Figs. 4 and 5. Moreover, the flow net shows the effects of the walls on the behavior of water flow. More information regarding the *TMVOC* simulator is included in the numerical simulation section.

Once the initial condition of each test was achieved and the pore water pressure reached a steady state, 800 mL (equivalent to 21,600 L in prototype) of the LNAPL was released through the orifice with a regulated flow in the model unit of ~0.45 mL/s. After the LNAPL was released, video recording and pore pressure measurements were performed to investigate the behavior of the LNAPL migration over a period of 128 min, which is equivalent to 80 days in prototype time.

Results and Discussions

The LNAPL was released to the soil surface at the center of the model and it rapidly spread over the surface of the model between the containment walls. The LNAPL then moved downward into the soil layer and was observed through the Plexiglas wall of the model container. In this study, the LNAPL migration was modeled as a 2D line source based on the observations during the centrifuge tests. This assumption was confirmed from the model dissection after the centrifuge test, where a consistent distribution of the LNAPL was observed throughout the cross section of the model.

Results from the centrifuge modeling and the numerical simulation of the LNAPL plume distribution at the end of all four experiments are shown in Fig. 6. The LNAPL plume migration of test 1 is shown in Fig. 6(a). The LNAPL plume migrated underneath the wall with a symmetrical plume distribution. In this case, the water level was significantly depressed because of the large volume of the LNAPL confined between the walls that resulted in a high positive-pressure build-up, as observed from the pore water-pressure measurement. As a result, the depth of the wall was inadequate for confining the LNAPL migration. The LNAPL plume migration of test 2 is shown in Fig. 6(c). Similar to test 1, the LNAPL plume migrated with a symmetrical plume distribution, but in this case, the depth of the wall was adequate for confining the LNAPL migration owing to the higher water level. The front of the LNAPL plume remained stable at the depth of 1.25 m below the initial water level.

The LNAPL plume migration of tests 3 and 4 is shown in Figs. 6(e and g), respectively. The LNAPL plume migrated with an asymmetric plume distribution because of the groundwater flow. In both tests 3 and 4, the LNAPL level at the higher pressure side of the model remained above the tip of the wall, whereas the LNAPL plume migrated underneath the wall at the lower pressure side of the model. The depression of water table was found to be larger in the case of water flow because of an advection effect. Comparing tests 3 and 4, the amount of the LNAPL plume migration underneath the wall increased as the pressure head difference increased. These results indicate that the depths of the soil-cement walls below the groundwater level should be no less than 1.50 m for no groundwater flow and 2.50 m for groundwater flow.

Pore Pressure Measurement

Variations of pore water pressure at various depths within the soil layer are presented in Fig. 7. During tests 1 and 2 (no groundwater flow), the water level decreased slightly at a constant rate because of the evaporation. The evaporation was not observed in tests 3 and 4 (groundwater flow) because the pumping system was capable of supplying water during the test.

Plots of the pore pressure change versus time for tests 1 and 2 are shown in Figs. 7(a and b), respectively. For test 1, the water level was maintained near the wall tip at the start of testing. When the LNAPL front reached sensors A1, C1, and A2 the pressure initially increased but then decreased after the LNAPL passed these sensors. Once the LNAPL reached sensors B2 and A3, the pressure increased, however, no pressure decrease was measured. This indicated that the LNAPL migration reached the initial water level and began depressing the water level. As a result of the water level depression, the LNAPL could migrate underneath the wall and spread laterally, which was observed from video recording. In this case, the depth of the wall below the water level was inadequate. In test 2, the LNAPL front reached all of the sensors except sensor B2, indicating that the LNAPL was stable above this location. The water level was depressed to a depth of 1.2 m corresponding to the location of sensor B1, where the pore pressure increased. In this case, the depth of the wall was adequate to contain the LNAPL migration. The pore pressure measurements agreed with the observations from video recording. In addition, there were no observations of pore pressure

J. Geotech. Geoenviron. Eng. 2013.139:892-902.

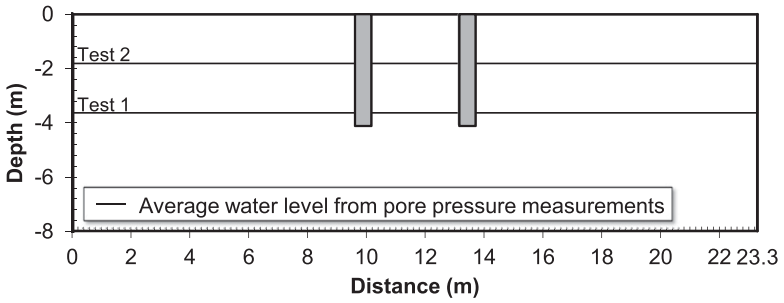

Fig. 3. The phreatic surface of groundwater for tests 1 and 2 from pore pressure measurements (prototype unit)

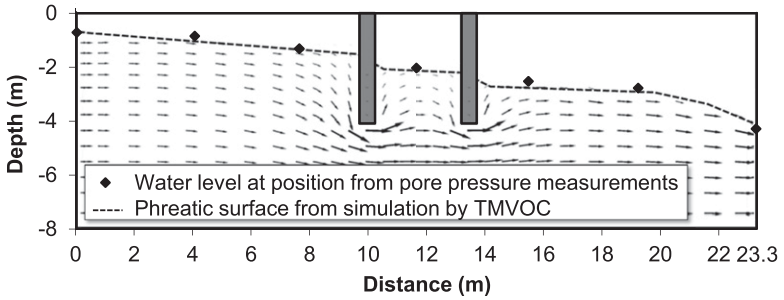

Fig. 4. Phreatic surface determination for test 3 comparing numerical simulation (*TMVOC*) and pore pressure measurements

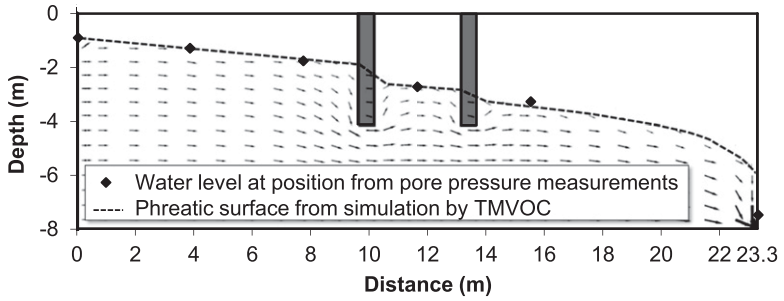

Fig. 5. Phreatic surface determination for test 4 comparing numerical simulation (*TMVOC*) and pore pressure measurements

change outside the wall indicating that the wall can act as an effective LNAPL containment barrier.

Plots of the pore pressure change with time for tests 3 and 4 are shown in Figs. 7(c and d), respectively. For test 3, the average water level within the containment was comparable to the water level in test 2, however, in test 3 the water level was depressed to 2.07 m, corresponding to the location of sensor A11. The depth of water depression in test 3 was greater than in test 2, and the observations from the video recording show that the LNAPL plume migrated underneath the wall at the lower pressure side of the model. In this case, the depth of the wall was inadequate. In test 4, an increased head difference resulted in a higher flow velocity and a slightly lower water pressure in the contained area. It was observed that the LNAPL front reached sensor A12, followed by sensors A11 and A3. In this test, the water depression was observed to be 2.9 m, resulting in the LNAPL migrating underneath the wall at the low-pressure side. The behavior observed in test 4 was similar to test 3, but the quantity of the LNAPL that migrated underneath the wall was greater than that in test 3. In addition, pore pressures at sensors A13, A14, and A15 fluctuated because of the high velocity of the groundwater flow. The pore pressure measurements provide a more detailed insight into the LNAPL migration behavior. Results from these measurements agreed well with the observations from the video recording.

Contours and Velocity of the Plume Movement

This section is focused on a comparison between cases of no groundwater flow (test 2) and groundwater flow (test 3). Snapshots of the plume migration obtained from the video recording at various times and each snapshot were processed using graphical software (*PhotoShopCS3*). The digitized perimeters of the plume were extracted to construct the contour of the LNAPL distribution with time, as shown in Fig. 8. This technique was used by Esposito et al. (1999, 2000) and Soga et al. (2003). Velocity of the front, measured from pore-pressure sensors, was calculated from the locations of the sensors and times when the plume movements reached the sensors, as shown Fig. 7. For test 2, the LNAPL plume reached the water level at 1.81 m below the wall within 20 days and the LNAPL was stable at ~0.99 m above the wall tip. For test 3, the LNAPL plume reached the higher pressure side water level at 1.93 m below the wall within 6 days. Sixty days after the LNAPL was released, the LNAPL plume migrated underneath the wall at the lower-pressure side.

J. Geotech. Geoenviron. Eng. 2013.139:892-902.

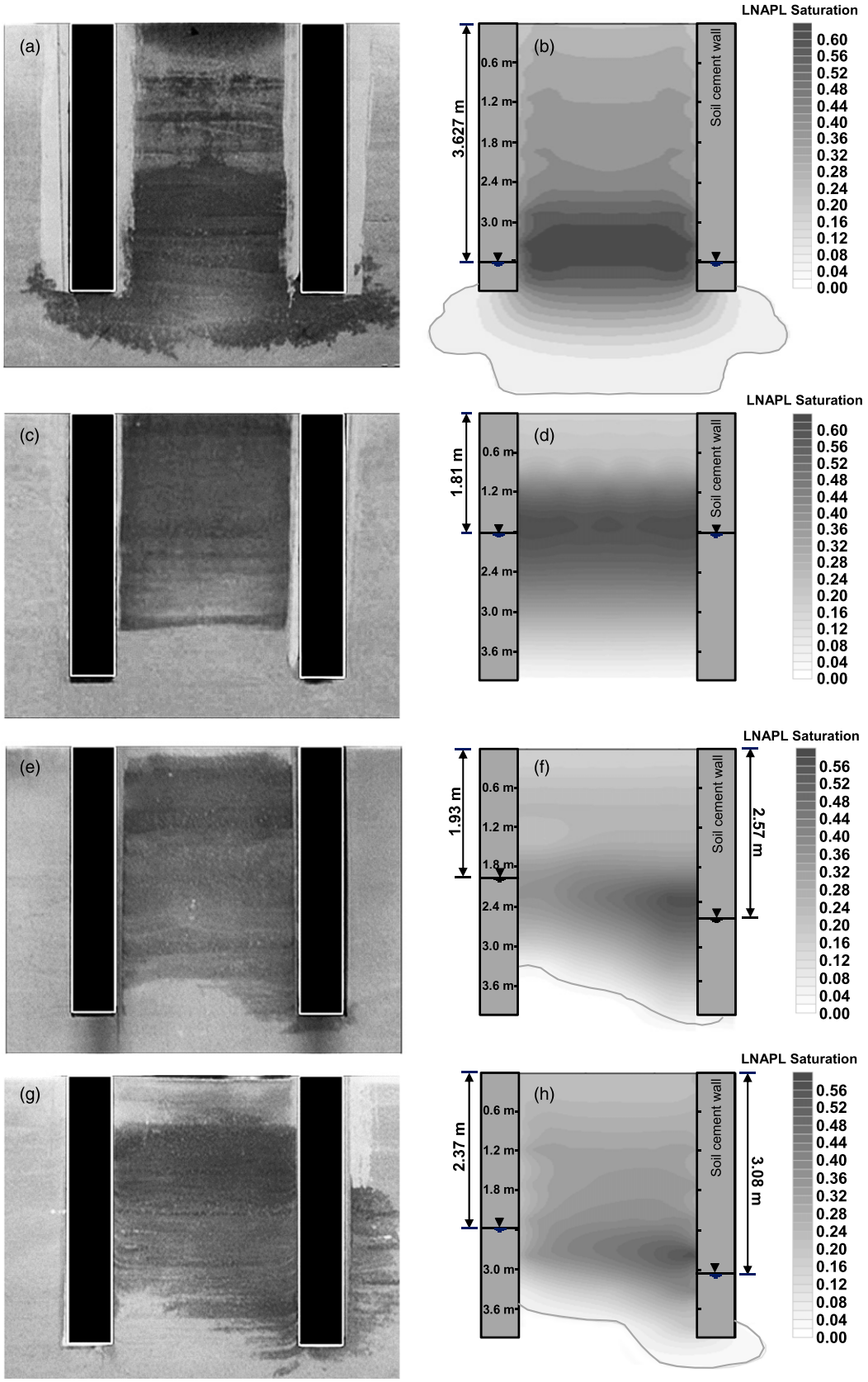

Fig. 6. LNAPL plume migration at the end of tests; (a) centrifuge test 1; (b) numerical simulation test 1; (c) centrifuge test 2; (d) numerical simulation test 2; (e) centrifuge test 3; (f) numerical simulation test 3; (g) centrifuge test 4; (h) numerical simulation test 4 (prototype unit)

J. Geotech. Geoenviron. Eng. 2013.139:892-902.

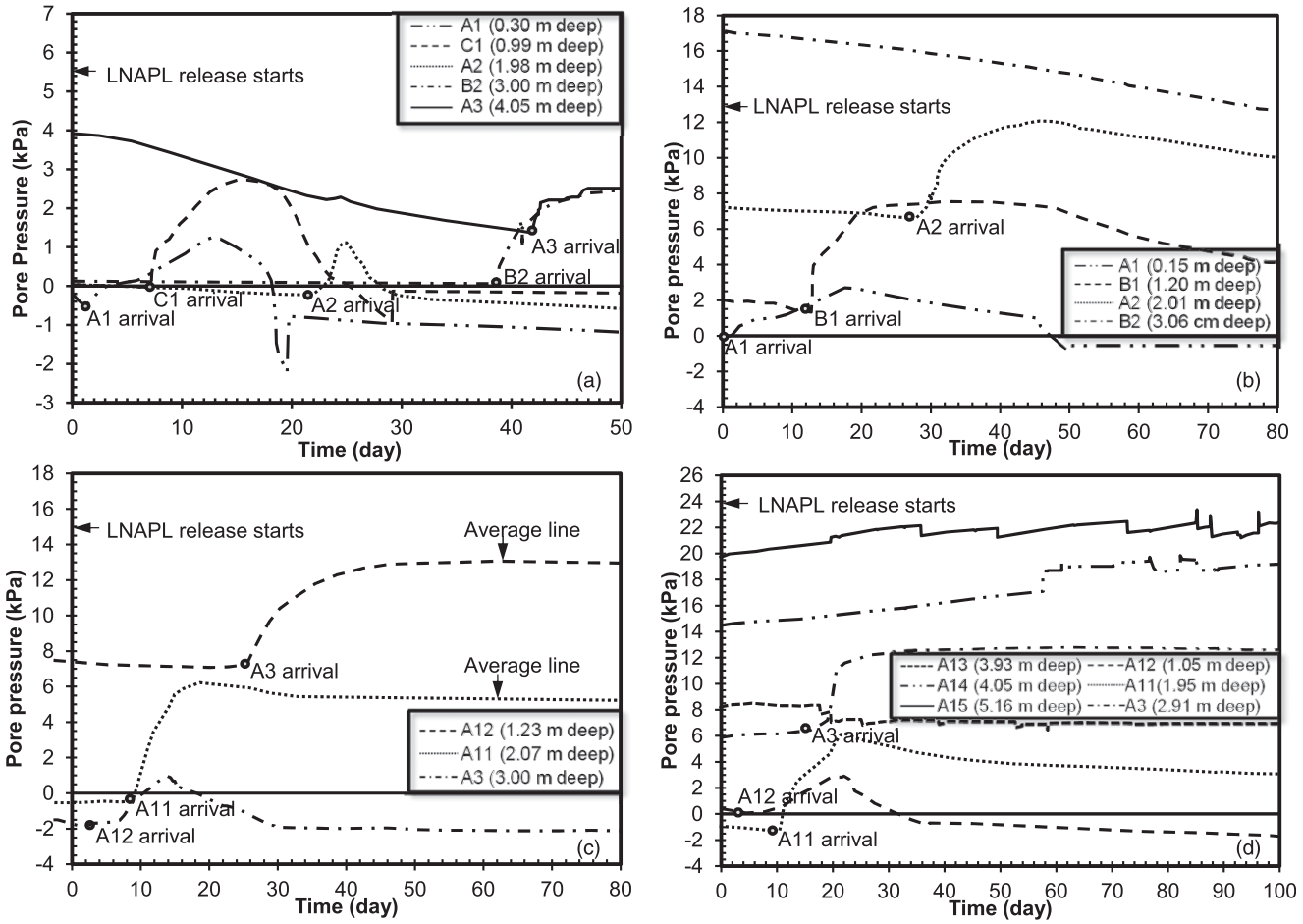

Fig. 7. Change in pore water as a function of time; (a) test 1; (b) test 2; (c) test 3; (d) test 4 (prototype unit)

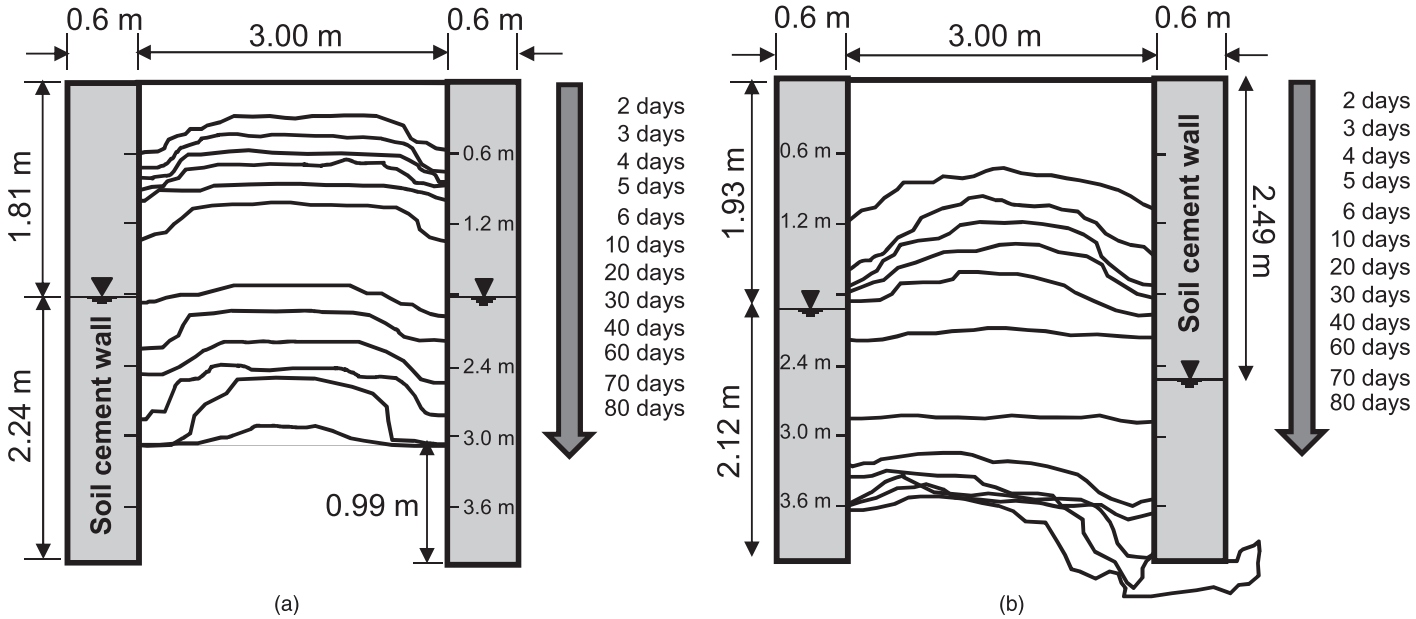

Fig. 8. Contours of LNAPL movement; (a) test 2; (b) test 3 (prototype unit)

J. Geotech. Geoenviron. Eng. 2013.139:892-902.

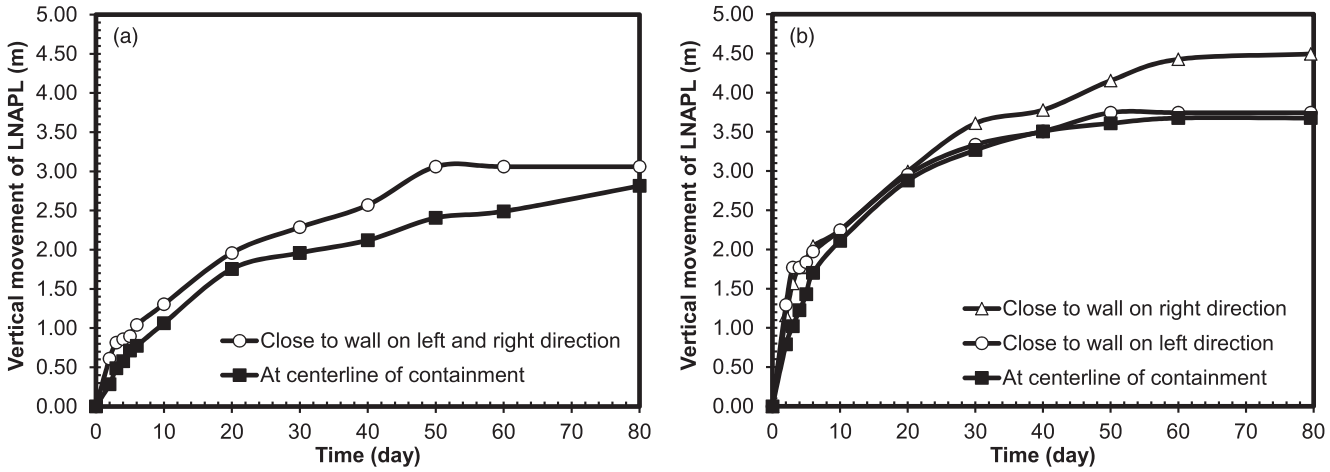

Fig. 9. Comparison of LNAPL movement at centerline and near the wall; (a) test 2; (b) test 3 (prototype unit)

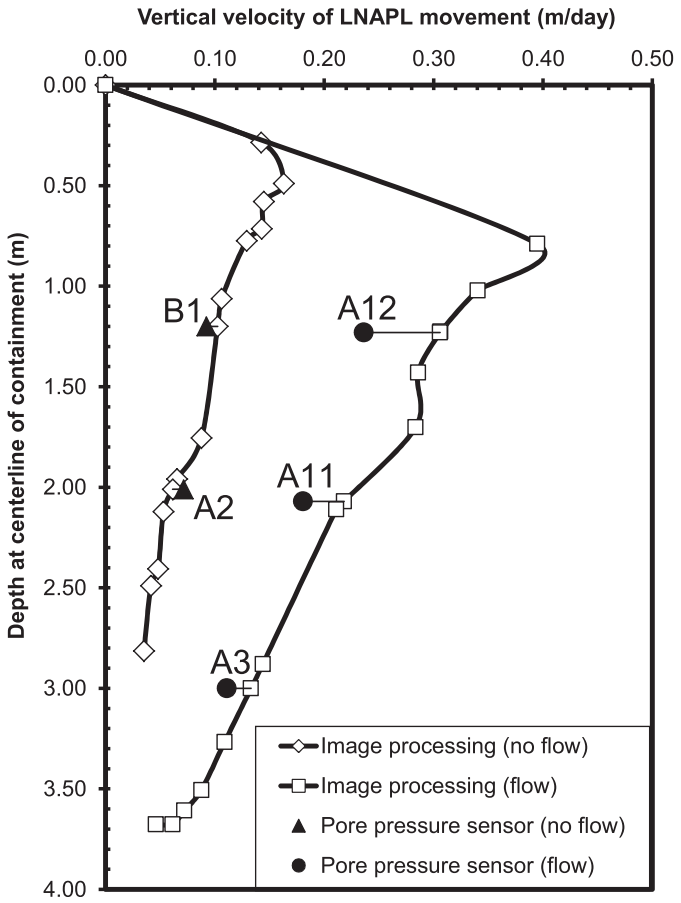

Fig. 10. Comparison of plume velocity (prototype unit)

The LNAPL plume distributions for both cases were examined from the vertical LNAPL movement versus times at the centerline and near the walls, as shown in Fig. 9. The LNAPL moved symmetrically downward for the case of no groundwater flow, as shown in Fig. 9(a). The LNAPL initially moved slightly faster near the walls than at the centerline, however, the front of the LNAPL plume near the walls and at the centerline stabilized at the same level. For the case of groundwater flow, the LNAPL moved asymmetrically downward and faster than the case of no groundwater flow, as shown in Fig. 9(b). The LNAPL near the wall at the lower-pressure side migrated faster than near the wall at the higher-pressure side because of the groundwater flow direction.

The distance at the centerline of the vertical plume movement at various times was used to calculate the velocity of the LNAPL migration and is presented in Fig. 10. The velocities of the front measured from the pore-pressure sensors were calculated from the sensor locations and the times at which the plume reached these locations, as plotted in Fig. 7. These velocities were compared with the velocities obtained from the image analysis presented in Fig. 8. The results from the pore pressure measurements were shown to be in general agreement with the image analysis. Some differences were observed for the case of groundwater flow and may be caused by the asymmetrical plume migration distribution. Overall, the plume velocity decreased with depth for both cases, and the plume velocity in the groundwater flow case was faster than that in the case with no groundwater flow.

Numerical Simulation Results

The numerical simulator utilized in this study is *TMVOC*, which was used within *PetraSim*. The *TMVOC* simulator is based on the code of *TOUGH2*, which was developed by Pruess and Battistelli (2002). Multiphase organic contaminant migration has been modeled using *TOUGH2* as the simulator by several authors, including Soga et al. (2003), Dunn (2005), Fagerlund et al. (2006), Fagerlund and Niemi (2007), Battistelli (2008), and Kererat and Soralump (2009b).

Input Model Parameters

The input parameters required for the numerical simulation are grouped into three sets as follows:

1. Properties of soil and soil cement, which are the particle density, the porosity, and the hydraulic conductivity, were the same as the properties of the experimental materials used in centrifuge test as described previously.
2. The air-water–saturation-capillary head (S-P) relationships of the tested soil and soil cement were based on tests conducted by Rungruang and Kererat (2010). The static two-phase S-P relationships of the soil and soil cement (NAPL-water and air-NAPL) were estimated from air-water–S-P relationships using a scaling-factor method proposed by Leverett (1941) and Parker et al. (1987), as shown in Fig. 11. The S-P relationships were used to estimate hydraulic conductivity function (k-S) using the Jackson (1972) equation. The model parameters for

J. Geotech. Geoenviron. Eng. 2013.139:892-902.

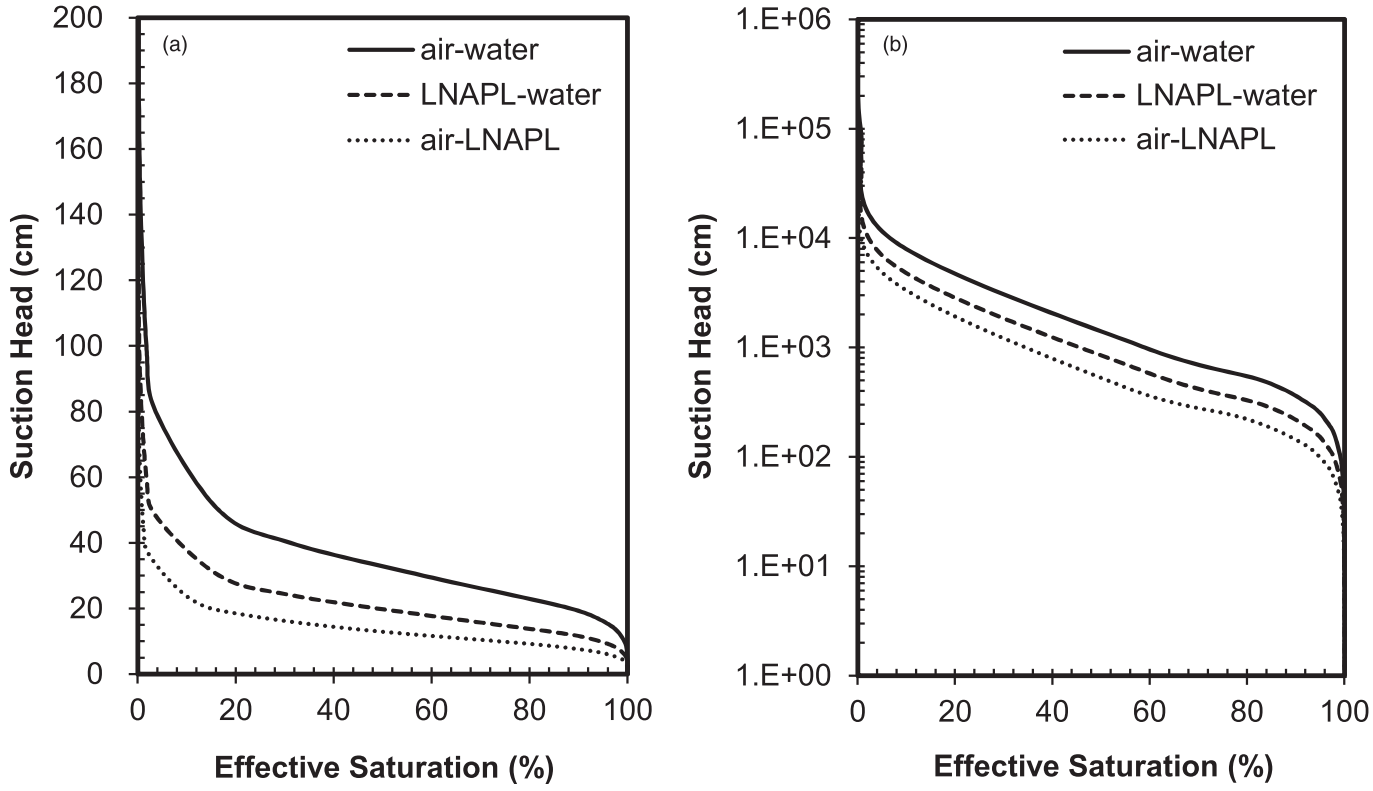

Fig. 11. Three two-phase scaled-saturation-capillary head (S-P) relationships; (a) sandy soil; (b) soil cement [data from Rungruang and Kererat (2010)]

the soil and soil cement were determined using the van Genuchten (1980) model and Parker et al. (1987) model to estimate the k-S-P relationships, as reported in Table 2.

3. Typical chemical properties of LNAPL were found in Reid et al. (1987). The LNAPL properties are comparable with the properties of liquid paraffin used in this study, as shown in Table 1.

Discretization, Initial, and Boundary Conditions

The two-dimensional sections of the numerical models were generated to replicate the cross sections of the centrifuge models. The groundwater levels measured from the centrifuge models were used as the side boundary conditions. The grid spacing of the numerical models, in the vertical and the horizontal directions, was based on the groundwater levels and the thickness of the containment. Simulations were performed under isothermal conditions. The atmospheric boundary condition was fixed at the grid top and specified as the constant absolute pressure of 1.013×10^5 Pa. A soil grain specific heat of 50,000 J/kg °C and a porosity of 0.999 were assumed for the atmospheric grid blocks because effects of the inner domain on the atmospheric boundary are negligible because of the volume of the atmospheric boundary (Rasmusson and Rasmusson 2009). The walls were modeled as low-permeability material. The simulated pore pressure distributions from the centrifuge tests were applied to the boundary condition and the model was run to reach the steady-state condition before the introduction of the LNAPL.

Validation of Numerical Results

The computed LNAPL saturation contours at the end of the testing are compared with the centrifuge test results as shown in Fig. 6. The numerical models simulated the observed effects of the water level and groundwater flow on the plume migration distribution. The LNAPL plume distributions of tests 1 and 2 are shown in Figs. 6(b and d), respectively. For test 1, the LNAPL plume distribution shows that the LNAPL can migrate underneath the wall. A large amount of the LNAPL was retained above the groundwater level, and some of the LNAPL was trapped in the unsaturated zone. The plume migration distribution was symmetrical, similar to the results of the centrifuge test. For test 2, the LNAPL plume distribution shows that the plume migration distribution was symmetrical. The LNAPL plume can penetrate below the groundwater level to a greater extent than that observed in the centrifuge test, however, the amount of the LNAPL near the wall tip was minimal. The LNAPL plume distributions of tests 3 and 4 are shown in Figs. 6(f and h), respectively. The plume migration was asymmetrical, similar to the centrifuge test results. The numerical simulation results show a large amount of the LNAPL accumulated at the lower-pressure side, and that the LNAPL could migrate underneath the wall. In this case, the LNAPL migrated underneath the wall to a lesser extent in the numerical simulation than in the centrifuge test. The various plume migration distributions in the numerical simulation and the centrifuge test results from an uncertainty in the capillary and the relative permeability parameters, including some of the chemical properties of the LNAPL. Overall, the results from the numerical simulations agreed with the results from the centrifuge experiments. Both methods confirmed the effective performance of the soil-cement wall as a containment barrier.

Conclusions

In this study, four centrifuge experiments were performed to simulate LNAPL migration in sandy soil and the effects of groundwater flow on the performance of soil-cement walls used as a containment barrier. Data from pore pressure measurements, along with video recordings, provided detailed insight into LNAPL migration behavior. In all tests,

J. Geotech. Geoenviron. Eng. 2013.139:892-902.

Table 2. Model Parameters for Tested Sandy Soil and Soil Cement

Description	Sandy soil	Soil cement
Relative permeability parameters for Parker's model (Parker et al. 1987)		
Limiting saturation S_m	0.345[a]	0.345[a]
Fitting parameter, n	3[c]	3[c]
Capillary pressure parameters for the van Genuchten's model (van Genuchten1980)		
$\lambda = m = 1-1/n$	0.770[d]	
Residual water saturation, S_{lr}	0.146[b]	
$1/P_0 = \alpha/\rho_w g$ $(1/\text{Pa}^{-1})$	3.400×10^{-4}	
Maximum value for capillary pressure, $P_{\max}$ (Pa)	4.215×10^{-4} [e]	
Satiated water saturation, S_{ls}	1[b]	
Capillary pressure parameters for Parker's model (Parker et al. 1987)		
Limiting saturation, S_m		0[b]
Fitting parameter, n		2.068[b]
Strength parameter for air-NAPL, $\alpha_{an} = \alpha \times \beta an$		0.330[f]
Strength parameter for NAPL-water, $\alpha_{nw} = \alpha \times \beta nw$		0.217[f]

Note: Strength parameter is the parameter describing the shape of the saturation-capillary head curve. α = curve fitting parameter; $\beta an(=\sigma_{aw}/\sigma_{an})$ = scaling factor for air-NAPL; $\beta nw[=1/(1-1/\beta_{an})]$ = scaling factor for NAPL water.

[a]Curve-fitting parameter of k-function curve.

[b]Curve-fitting parameter of S-P curve.

[c]Recommended by Rasmusson and Rasmusson (2009).

[d]Calculated from van Genuchten curve fitting parameter (n).

[e]Measured from a suction test by Rungruang and Kererat (2010).

[f]Calculated from a fitting parameter multiplied by a scaling factor (Rasmusson and Rasmusson 2009).

the water level was depressed because of the large volume of LNAPL confined between the walls. In the case of no groundwater flow, the LNAPL migrated below the water level with a symmetrical plume distribution. In the case of groundwater flow, the LNAPL migrated at a faster rate and deeper below the initial water level compared with the case of no groundwater flow. The amount of the LNAPL migration below the initial water level increased as the pressure head difference increased for the case of groundwater flow. Based on this study, the depth of the soil-cement wall below the water level should be no less than 1.50 m for the conditions of no groundwater flow and 2.50 m for the conditions of groundwater flow. The LNAPL did not migrate through the soil-cement wall, indicating that the walls were effective as a containment barrier. Results from numerical simulations were in a good agreement with those from the centrifuge experiments.

Acknowledgments

The authors thank the Office of the Higher Education Commission, Thailand for the grant fund support under the program Strategic Scholarships for Frontier Research Network for the Joint Ph.D. Program Thai Doctoral degree for this research. The authors also thank Rajamangala Univ. of Technology Rattanakosin for providing funding for this research. Furthermore, thanks to staff of the Rensselaer Polytechnic Institute centrifuge laboratory for their help with the model design and testing.

References

Arulanandan, K., Thompson, P. Y., Kutter, B. L., Meegoda, N. J., Muraleetharan, K. K., and Yogachandran, C. (1988). "Centrifuge modeling of transport processes for pollutants in soils." *J. Geotech. Eng.*, 114(2), 185–205.

Battistelli, A. (2008). "Modeling multiphase organic spills in coastal sites with *TMVOC* V.2.0." *Vadose Zone J.*, 3(7), 875–883.

Bruce, D. A. (2000). "An introduction to the deep soil mixing methods as used in geotechnical applications." *Rep. FHWA-RD-99-138*, U.S. Department of Transportation, McLean, VA.

Dunn, A. M. (2005). "Air and LNAPL entrapment in the partially saturated fringe: Laboratory and numerical investigations." Ph.D. thesis, Univ. Notre Dame, Notre Dame, IN.

Esposito, G., Allersma, H. G. B., and Selvadurai, A. P. S. (1999). "Centrifuge modeling of LNAPL transport in partially saturated sand." *J. Geotech. Geoenviron. Eng.*, 125(12), 1066–1071.

Esposito, G. M., Allersma, H. G. B., Soga, K., Kechavarzi, C., and Coumoulos, H. (2000). "Centrifuge simulation of LNAPL infiltration in partially saturated porous granular medium." *Proc., Int. Symp. on Physical Modelling and Testing in Env. Geotech.*, Laboratoire Central des Ponts et Chaussées (LCPC), La Baule, France, 141–148.

Fagerlund, F., and Niemi, A. (2007). "A partially coupled, fraction-by-fraction modelling approach to the subsurface migration of gasoline spills." *J. Contam. Hydrol.*, 89(3–4), 174–198.

Fagerlund, F., Niemi, A., and Odén, M. (2006). "Comparison of relative permeability –fluid satuartion – capillary pressure relations in the modeling of non-aqueous phase liquid infiltration in variably saturated, layered media." *Adv. Water Resour.*, 29(11), 1705–1730.

Garnier, J., et al. (2007). "Catalogue of scaling laws and similitude questions in geotechnical centrifuge modeling." *Int. J. Phys. Model. Geotech.*, 7(3), 1–23.

Gazaway, H. N., and Jasperse, B. H. (1992). "Jet grouting in contaminated soils." *Proc., Grouting, Soil Improvement and Geosynthetics (GSP 30)*, ASCE, Reston, VA, 206–214.

Hayashi, Y., and Allersma, H. G. B. (2004). "Centrifuge modelling of LNAPL transport in sand deposit by groundwater flow." *Proc., 14th Int. Conf. on Offshore and Polar Engineering*, Vol. 3, Int. Society of Offshore and Polar Engineers (ISOPE), Cupertino, CA, 464–469.

Hu, L. M., Lo, I. M. C., and Meegoda, J. N. (2006). "Centrifuge testing of LNAPL migration and soil vapor extraction for soil remediation." *Pract. Period. Hazard. Toxic Radioact. Waste Manage.*, 10(1), 33–40.

Illangasekare, T. H., Al-Sheridda, Z. M., and Reible, D. D. (1991). "Multiphase flow in porous media." *Proc., Centrifuge 91*, Balkema, Rotterdam, Netherlands, 517–523.

Jackson, R. D. (1972). "On calculation of hydraulic conductivity." *Sci. Soc. Am. Proc.*, 36(2), 380–382.

Kamon, M., Li, Y., Flores, G., Endo, K., Inui, T., and Katsumi, T. (2006). "Experimental and numerical study on migration of LNAPL under the influence of fluctuating water table in subsurface." *Annuals of Disas. Prev. Res. Inst.*, 49(B), 383–392.

Kererat, C., and Chaikaew, C. (2009a). "Suitable of soil cement mixing for containing contaminant migration." *Res. Rep. 2009*, Institute for Research and Development (IRD), Rajamangala Univ. of Technology Rattanakosin, Nakorn Pathom, Thailand.

Kererat, C., and Soralump, S. (2009b). "LNAPL migration through soil cement barrier with and without flow condition." *J. Energy Eng.*, 10(3), 185–193.

Leverett, M. C. (1941). "Capillary behavior in porous solids." *Trans. Am. Inst. Min. Metall. Pet. Eng.*, 142, 152–169.

Lo, I. M. C., Hu, L. M., and Meegoda, J. N. (2004). "Centrifuge modeling of light nonaqueous phase liquids transport in unsaturated soils." *J. Geotech. Geoenviron. Eng.*, 130(5), 535–539.

Nicholson, P. J., Jasperse, B. H., and Fisher, M. J. (1997). "Economic alternatives for containment barriers." *Int. Containment Tech. Conf. and Exhibit*, Institute for International Cooperative Environmental Research (IICER), St. Petersburg, FL.

J. Geotech. Geoenviron. Eng. 2013.139:892-902.

Parker, J. C., Lenhard, R. J., and Kuppusamy, T. (1987). "A parametric model for constitutive properties governing multiphase flow in porous media." *Water Resour. Res.*, 23(4), 618–624.

Pruess, K., and Battistelli, A. (2002). "*TMVOC*, a numerical simulator for three phase non-isothermal flows of multicomponent hydrocarbon mixtures in saturated–unsaturated heterogeneous media." *LBNL-49375*, Lawrence Berkeley National Laboratory, Berkeley, CA.

Rasmusson, K., and Rasmusson, M. (2009). "NAPL spill modeling and simulation of pumping remediation." M.S. thesis, Uppsala Univ., Uppsala, Sweden.

Reid, R. C., Prausnitz, J. M., and Poling, B. E. (1987). *The properties of gases and liquids*, McGraw Hill, New York.

Rungruang, S., and Kererat, C. (2010). "Contaminant migration behavior through soil cement barrier under full scale test." *Res. Rep. 2010*, Institute for Research and Development (IRD), Rajamangala Univ. of Technology Rattanakosin, Nakorn Pathom, Thailand.

Soga, K., Kawabata, J., Kechavarzi, C., Coumoulos, H., and Waduge, W. A. P. (2003). "Centrifuge modeling of nonaqueous phase liquid movement and entrapment in unsaturated layered soils." *J. Geotech. Geoenviron. Eng.*, 129(2), 173–182.

Sripongphichit, W. (2006). "Investigation of fossil fuel contamination in unsaturated zone using digital image analysis." M.E. thesis, Univ. of Kasetsart, Bangkok, Thailand.

Taylor, R. N. (1995). *Geotechnical centrifuge technology*, Chapman and Hall, London.

van Genuchten, M. T. (1980). "A closed-form equation for predicting the hydraulic conductivity of unsaturated soils." *Soil Sci. Soc. Am. J.*, 44, 892–898.

J. Geotech. Geoenviron. Eng. 2013.139:892-902.